Heliyon 10 (2024) e27217

Contents lists available at ScienceDirect

Heliyon

journal homepage: www.cell.com/heliyon

Research article

Trilobolide-6-O-isobutyrate exerts anti-tumor effects on cholangiocarcinoma cells through inhibiting JAK/STAT3 signaling pathway

Hao-Xuan Zhang [a,1], Rui Fan [a,1], Qian-En Chen [a,1], Lin-Jun Zhang [a], Yang Hui [b], Peng Xu [a], Si-Yang Li [a], Guang-Ying Chen [b,**], Wen-Hao Chen [b,***], Dong-Yan Shen [a,*]

[a] School of Medicine, Xiamen University, The First Affiliated Hospital of Xiamen University, Xiamen, 361003, China
[b] Key Laboratory of Tropical Medicinal Resource Chemistry of Ministry of Education, Hainan Normal University, Haikou, 570100, China

ARTICLE INFO

Keywords:
TBB
Cholangiocarcinoma
Proliferation
Apoptosis
JAK/STAT pathway

ABSTRACT

Trilobolide-6-O-isobutyrate exhibits significant antitumor effects on cholangiocarcinoma (CCA) cells by effectively inhibiting the JAK/STAT3 signaling pathway. This study aims to investigate the mechanisms underlying the antitumor properties of trilobolide-6-O-isobutyrate, and to explore its potential as a therapeutic agent for CCA. This study illustrates that trilobolide-6-O-isobutyrate efficiently suppresses CCA cell proliferation in a dose- and time-dependent manner. Furthermore, trilobolide-6-O-isobutyrate stimulates the production of reactive oxygen species, leading to oxidative stress and initiation of apoptosis via the activation of the mitochondrial pathway. Data from xenograft tumor assays in nude mice confirms that TBB inhibits tumor growth, and that there are no obvious toxic effects or side effects *in vivo*. Mechanistically, trilobolide-6-O-isobutyrate exerts antitumor effects by inhibiting STAT3 transcriptional activation, reducing PCNA and Bcl-2 expression, and increasing P21 expression. These findings emphasizes the potential of trilobolide-6-O-isobutyrate as a promising therapeutic candidate for the treatment of CCA.

1. Introduction

Cholangiocarcinoma (CCA) originates from various epithelial cells, including intrahepatic, perihilar, and distal bile ducts, and is a highly malignant tumor [1]. Each subtype of CCA has different biological characteristics, prognoses, and clinical treatment [2]. It is associated with many factors, including abnormal cell proliferation and a complicated tumor microenvironment [3–6]. The progression of CCA is driven by the anomalous activation of multiple signaling pathways [7–11], ultimately facilitating uncontrolled tumor growth and metastasis. Moreover, patients with CCA always have a poor prognosis [12,13], owing to drug resistance [14], and this problem has not yet been addressed worldwide, making it difficult to treat CCA. Therefore, it is necessary to explore new drugs for the treatment of CCA.

* Corresponding author.
** Corresponding author.
*** Corresponding author.
E-mail addresses: chgying123@163.com (G.-Y. Chen), chenwh04@163.com (W.-H. Chen), shendongyan@163.com (D.-Y. Shen).
[1] Hao-Xuan Zhang, Rui Fan and Qian-En Chen contributed equally to this work.

https://doi.org/10.1016/j.heliyon.2024.e27217
Received 11 August 2023; Received in revised form 23 February 2024; Accepted 26 February 2024
Available online 28 February 2024

Abbreviations

TBB	Trilobolide-6-O-isobutyrate
CCA	Cholangiocarcinoma

There is great promise in developing new anti-tumor drugs from natural plants [15], and the isolation of antitumor substances from plants that are effective and have low toxicity has been a hot topic for scholars globally [16,17]. More than 3000 Chinese herbs have been screened for cancer in China [18]. *Wedelia trilobata* is a traditional herb widely used in Chinese folk medicine. An increasing amount of evidence indicates that *Wedelia trilobata* possesses anti-inflammatory, antitumor, and antiviral effects [19–21], however, in-depth studies on the effective components extracted from *Wedelia trilobata* are lacking [22–24]. Trilobolide-6-O-isobutyrate (TBB) is an effective substance in *Wedelia trilobata*, consisting of one hydroxyl, two acetoxy, and one isobutyloxy group. It serves as a chemotherapeutic drug for the treatment of liver cancer by inhibiting the JAK/STAT3 pathway [25]. However, there have been no reports on the antitumor effect and mechanism of TBB in other tumors, and the role of TBB in the progression of CCA remains unclear.

Previous studies have demonstrated that TBB could be associated with antitumor effects by interfering with the JAK signaling pathway. Therefore, we hypothesize that TBB also exerts antitumor effects in CCA by inhibiting the JAK-STAT3 signaling pathway. We aim to understand whether TBB plays an effective antitumor role in the progression of CCA by examining its effects on the proliferation, cycling, and apoptosis of CCA cells and to study its mechanism of action. This study is the first to investigate the inhibitory effect of TBB on CCA, which can provide evidence of the medicinal value of TBB and establish a foundation for further CCA treatment.

2. Materials and methods

2.1. Reagents and antibodies

Trilobolide-6-O-isobutyrate was provided by Wen-Hao Chen, Professor of Chemistry and Chemical Engineering, Hainan Normal University, China. The Roswell Park Memorial Institute (RPMI)-1640 medium, 0.25% trypsin-ethylenediaminetetraacetic acid, 100 × penicillin/streptomycin, and fetal bovine serum (FBS) were obtained from Gibco (Rockville, MD, USA). The hematoxylin and eosin staining kit, Hoechst 33,258 staining kit, and crystal violet were obtained from Solarbio (Beijing, China). The MTS assay kit was purchased from Promega (Madison, WI, USA). Propidium iodide (PI), z-VAD-fmk, and Annexin V-FITC apoptosis detection kit were obtained from Abcam (Cambridge, UK). An acridine orange/ethidium bromide (AO/EB) staining kit was obtained from Sangon Biotech (Shanghai, China). 5-Ethynyl-2′-deoxyuridine (EdU) cell proliferation detection kit was obtained from RiboBio (Guangzhou, China). Caspase-3 activity assay kit, antibody stripping buffer and reactive oxygen species (ROS) detection kit were obtained from Beyotime Biotechnology (Shanghai, China). Antibodies against caspase-3, P21, Ki67, Bcl-2, PARP, CyclinB1, CyclinE, and PCNA were obtained from Santa Cruz Biotechnology (Shanghai, China), Bax came from Proteintech (Wuhan, China), β-catenin, GAPDH, p-STAT3 and STAT3 came from Cell Signaling Technology (Shanghai, China). An environmentally friendly transparent agent was purchased from Huntz Biotech Co. (Wuhan, China). A DAB kit was obtained from ZSGB BIO (Beijing, China), and 5-fluorouracil (5FU) was purchased from Shanghai Macklin Biochemical Co. (Shanghai, China).

2.2. Extraction, isolation and purity of TBB

Trilobolide-6-O-isobutyrate was extracted and isolated from *Wedelia trilobata*, and the chemical structure of TBB (Fig. 1A) contains hydroxyl, acetoxy, and isobutyloxy groups according to a previous study [25,26]. The purity of TBB was determined using high-performance liquid chromatography (HPLC), which yielded a range of 97.43–98.47% purity (Fig. 1B).

2.3. Cell culture and treatment

QBC939 cells were provided by Professor Shu-Guang Wang of the Southwest Hepatobiliary Hospital, Third Military Medical University, Chongqing, China. TFK-1, HuCCT-1, and MZ-ChA-1 cells were obtained from the Chun-Dong Yu Laboratory at Xiamen University, Xiamen, China. TFK-1 was cultured in the Dulbecco's Modified Eagle medium, and the other three CCA cells were cultured in the RPMI-1640 medium supplemented with 100 × penicillin/streptomycin solution and 10% FBS under a humidified atmosphere containing 5% CO2 at 37 °C [27], and treated with TBB, which was extracted from *Wedelia trilobata* in various concentrations.

2.4. Cell viability analysis and cytotoxicity tests

Cholangiocarcinoma cells were seeded in 96-well plates at a density of 5000 cells per hole, and incubated at 37 °C for 24 h. Subsequently, the cells were treated with varying concentrations of TBB for 24 h or 48 h. Additionally, MTS [28] was used to measure cell viability and cytotoxicity, according to the manufacturer's instructions. An MTS reagent was added directly to the wells, which were incubated for 1–4 h, and the absorbance at 490 nm was recorded on a 96-well plate reader. Absorbance measured at 490 nm was directly proportional to the number of viable cells in the culture.

A

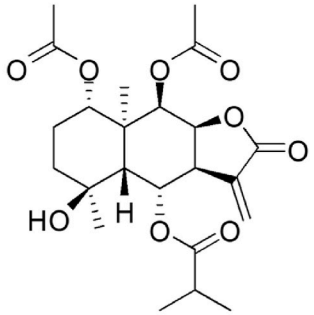

B

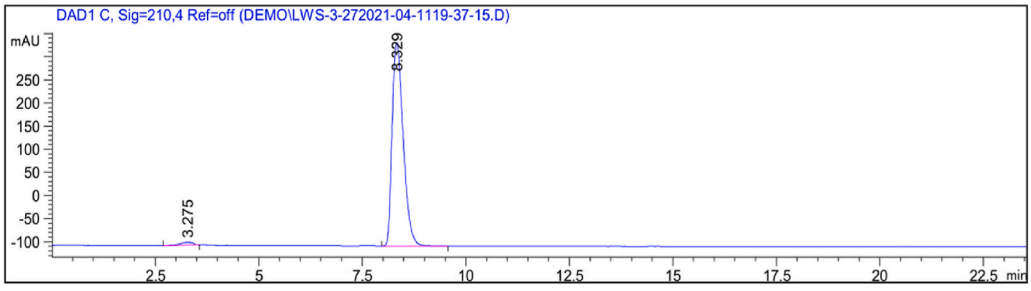

No.	RT	type	Peak Width	Peak Area	Peak Height	Peak Area
#	[min]		[min]	[mAU*s]	[mAU]	%
1	3.275	BB	0.2967	126.96576	5.81580	1.5257
2	8.329	BB	0.2915	8194.71094	439.58182	98.4743

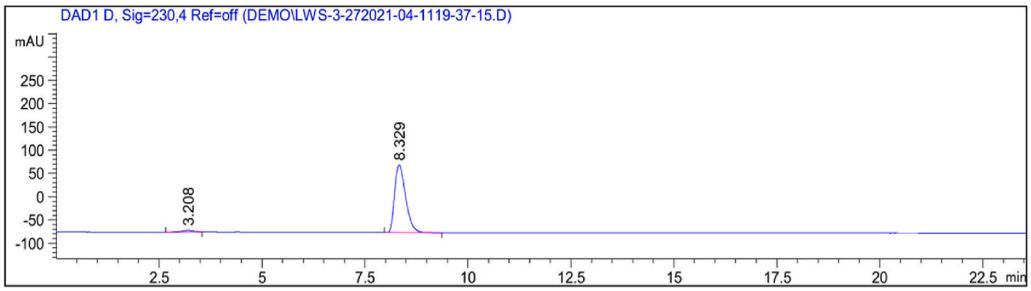

No.	RT	type	Peak Width	Peak Area	Peak Height	Peak Area
#	[min]		[min]	[mAU*s]	[mAU]	%
1	3.208	BB	0.2981	71.24771	3.40519	2.5710
2	8.329	BB	0.2913	2699.98975	144.95490	97.4290

Fig. 1. Detection of the Structure and Purity of TBB.
(A) Chemical structure of TBB. (B) HPLC chromatogram of TBB at the detection wavelength of 210 nm (up) and 230 nm (down).

2.5. Cell colony formation assay

The CCA cells were digested, seeded in six-well plates (1000/wells) and treated with different concentrations of TBB for two weeks. The CCA cells were immobilized with absolute ethanol and treated with crystal violet at room temperature for 15 min. After drying, the cell number and colony formation rate of each well were photographed and quantified using ImageJ software [29].

2.6. Hoechst staining

Hoechst is a specific dye that crosses cell membranes and binds double-stranded DNA to produce blue fluorescence. Chromatin in the nucleus exhibits bright and strong blue fluorescence during apoptosis. In the study, six-well plates were used to culture the CCA cells, which was performed with TBB at 2.5 μM and 5 μM for another 24 h after a night. The CCA cells were stained with Hoechst at room temperature for 5 min. The staining solution was discarded, and the cells were washed twice with phosphate buffered saline (PBS) before being observed and photographed under a fluorescence microscope [30].

2.7. EdU assay

5-Ethynyl-2′-deoxyuridine is a new analog of thymidine, and thymine is replaced with DNA, which is newly synthesized during DNA synthesis. The EdU acetylene group can form a stable triazole ring structure through a covalent reaction with an azide labeled by fluorescence. Therefore, newly synthesized DNA could be detected using a luciferin-labeled azide. 5-Ethynyl-2′-deoxyuridine can be used as a fuel to detect cell proliferation [31]. The CCA cells were digested and seeded in 96-well plates overnight. After treatment with TBB of various concentrations for another 24 h, the EdU was incubated with CCA cells at 37 °C for 2 h, and then fixed with absolute ethanol for 15 min. After permeabilization of CCA cells with 0.5% Triton-X-100, Hoechst 33,258 was used to stain the nuclei. Finally, the fluorescence of CCA cells was observed under a microscope.

2.8. Western blot

The CCA cells were treated with various concentrations of TBB and lysed in radioimmunoprecipitation assay buffer. Sodium dodecyl-sulfate polyacrylamide gel electrophoresis was used to separate the proteins and polyvinylidene difluoride (PVDF) membranes were used for their transfer. After blocking with 5% skim milk at room temperature, the PVDF membranes were cut horizontally, with at least two markers around the indicated proteins. Next, the membranes were incubated with indicated primary antibodies for one night at 4 °C, after the treatment with the secondary antibodies for 1 h at room temperature, the expression of proteins was visualized by enhanced chemiluminescence. For proteins of similar molecular weights, the membranes were stripped using an antibody stripping buffer [32] at room temperature for 10 min after the first visualization, and the membranes were blocked with 5% skim milk, another primary antibody, secondary antibody incubation, and protein visualization.

2.9. Cell cycle analysis

Propidine iodide is an analog of ethidium bromide that can be embedded in nuclear DNA to make the cell fluoresce red. Based on the intensity of cell fluorescence, we determine the amount of DNA and deduce the cell cycle [33]. The CCA cells were cultured in six-well plates, maintained at 5 × 105 cells/well for 24 h, and incubated with TBB at different concentrations for another 24 h. All the cells were collected and immobilized with 75% ethanol for 12 h at 4 °C, then the CCA cells were washed twice by PBS and placed on ice after treating with RNase A in 37 °C for 30 min. Additionally. 10 μL of PI was used to stain the CCA cells at 4 °C in the dark for 10 min. Next, the cell cycle was analyzed using flow cytometry (FCM). The results are presented using ModFit LT software.

2.10. Annexin V-FITC/PI staining

Phosphatidylserine overturns from the inside to the outside of the cell membrane during the early stages of apoptosis. Annexin V was labeled with FITC, a green fluorescent probe, which has a specific affinity for phosphatidylserine. Due to the loss of cell membrane integrity, PI is embedded in the nucleus and emits red fluorescence at the late stage of apoptosis. Apoptosis can be detected by double staining with two dyes [34]. In this study, TBB was added to each group with different concentrations for another 24 h after incubating the CCA cells at a density of 1×10^5 cells per hole at 37 °C for 24 h. All the CCA cells were stained with Annexin V-FITC for 20 min at room temperature and PI at 4 °C for 5 min in the dark, and FCM was then employed to evaluate apoptosis.

2.11. Casepase-3 activity detection

Caspase 3 catalyzes the production of yellow *p*-nitroaniline (pNA) from the substrate acetyl-Asp-Glu-Val-Asp *p*-nitroanilide (Ac-DEVD-pNA), which allows the detection of caspase-3 activity by measuring absorbance [35]. However, pNA has strong absorption near 405 nm. The CCA cells were treated with various concentrations of TBB in the presence of the apoptosis inhibitor, z-VAD-fmk. Next, the cells were lysed using the lysis solution from the kit for 15 min, centrifuged, and the supernatant was transferred to a pre-cooled centrifuge tube. Then AC-DEVD-PNA (2 mM) was incubated with protein at 37 °C for 60–120 min, and the absorbance was detected at 405 nm.

2.12. ROS

The reactive oxygen assay kit was used to detect cellular levels of ROS [36]. Approximately 5 × 105 cells per hole were cultured in six-well plates for 24 h, and various concentrations of TBB were added for another 24 h. 2′,7′-Dichlorodihydrofluorescein diacetate (DCFH-DA) was diluted with serum-free culture medium in a ratio of 1–1000. The cells were collected and suspended in diluted

DCFH-DA and incubated for 20 min at 37 °C in a cell culture incubator. Mixing was performed upside down every 3–5 min to ensure full contact between the probe and cells. The cells were washed three times with serum-free cell culture medium to adequately remove DCFH-DA that had not entered them. Finally, the cells were collected, sieved through a 400 mesh, and ROS production of cells ROS were tested by FCM.

2.13. AO/EB staining

Acridine orange/ethidium bromide double staining is commonly used to detect apoptosis detection [37]. Acridine orange is membrane permeable, and can pass through normal cells to stain the cell nucleus with a uniform green fluorescence. Ethidium bromide can only pass through incomplete cell membranes and enter dead cells to stain the nucleus orange-red, so that normal, apoptotic, and necrotic cells can be distinguished by staining. Six-well plates were seeded in the CCA cells for 24 h and treated with different concentrations of TBB for another 24 h. The AO/EB working solution was prepared and incubated with the CCA cells at room temperature, and the fluorescence signals of the CCA cells were observed under a microscope.

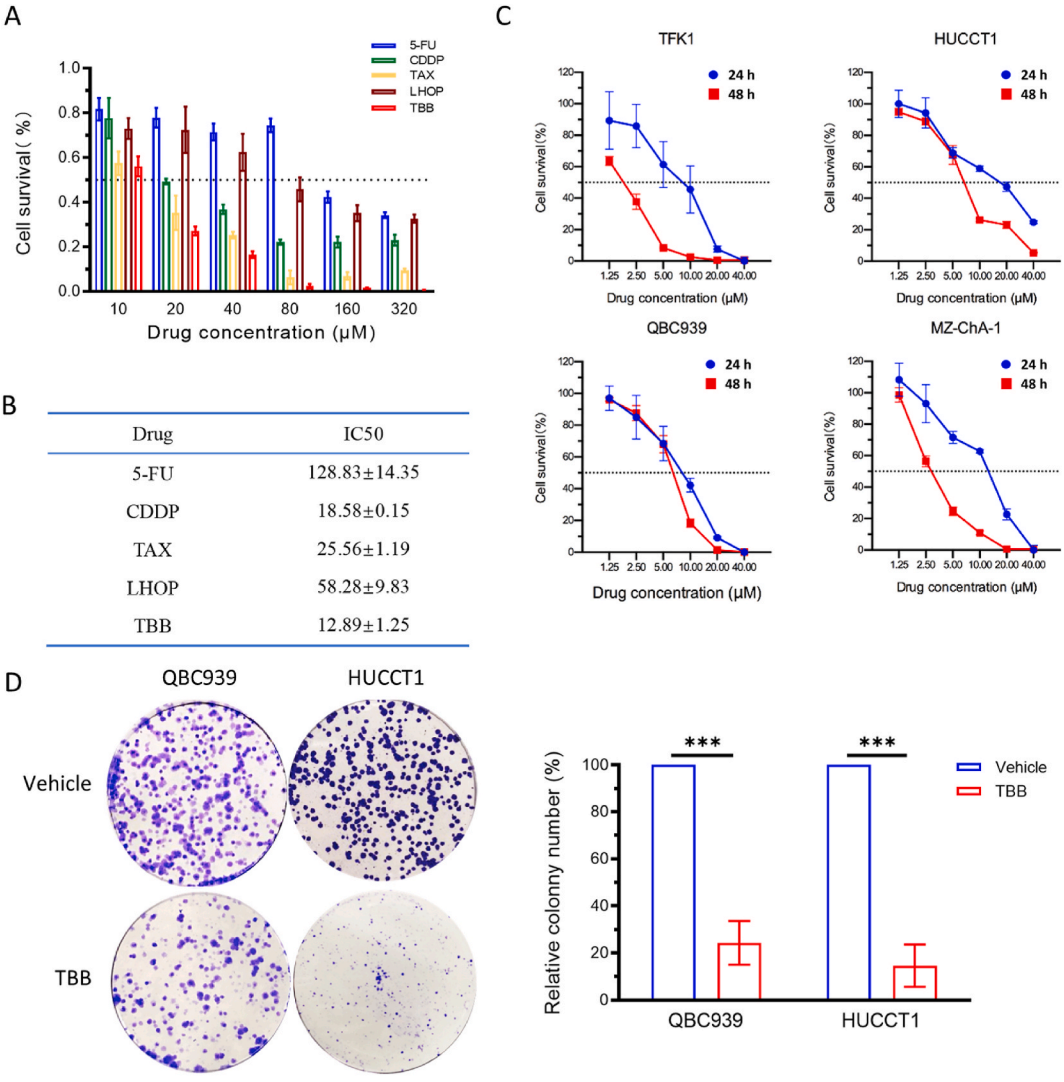

Drug	IC50
5-FU	128.83±14.35
CDDP	18.58±0.15
TAX	25.56±1.19
LHOP	58.28±9.83
TBB	12.89±1.25

Fig. 2. Inhibitory effect of TBB on CCA cell survival and colony formation
(A) Cell survival rate was measured by MTS assay in QBC939 cells, which were treated with 5-FU, CDDP, TAX, LHOP, and TBB at different concentrations (10 μM, 20 μM, 40 μM, and 80 μM) for 24 h. (B) IC50 of five drugs. (C) The percentage of cell survival was measured by MTS assay in TFK1, HuCCT1, QBC939, and MZ-ChA-1 cells, which were treated with TBB at different concentrations (1.25 μM, 2.5 μM, 5 μM, 10 μM, 20 μM, and 40 μM) for 24 h and 48 h. (D) The ability of colony formation was detected in QBC939 and HuCCT1 cells treated with TBB at 5 μM, and the relative number of colony formation was quantified. The expression of data values was indicated as mean ± SEM of three independent experiments. *P < 0.05, **P < 0.01, and ***P < 0.001.

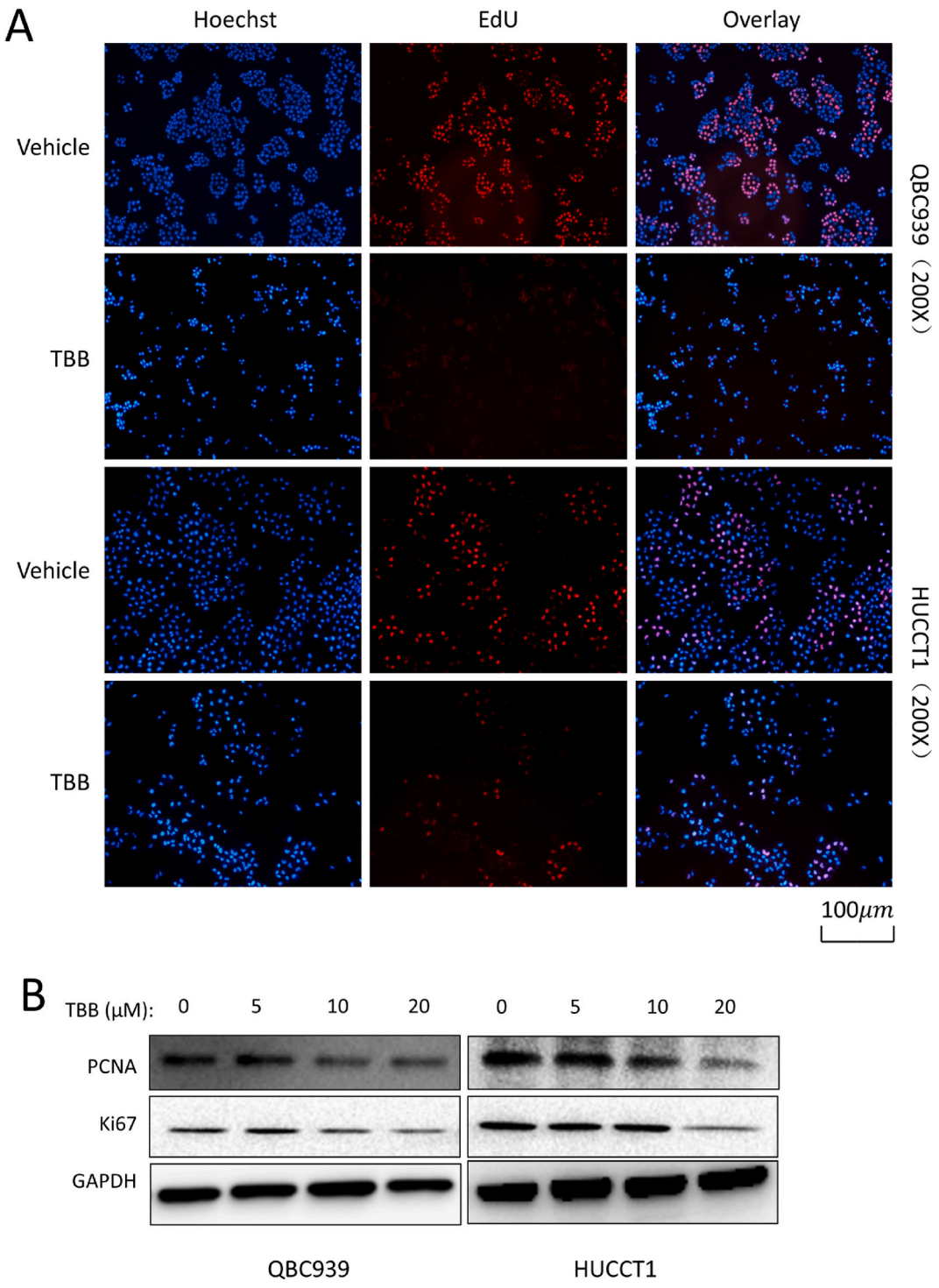

Fig. 3. TBB inhibited the proliferation of QBC939 and HuCCT1 cells.
(A) The efficiency of TBB on proliferation was assessed by Hoechst 33,258 and EdU staining in QBC939 and HuCCT1 cells treated with TBB at 5 μM for 24 h. (B) The expression of proliferation protein was detected using western blotting in QBC939 and HuCCT1 cells treated with TBB at various concentrations (0 μM, 5 μM, 10 μM, and 20 μM) for 24 h.

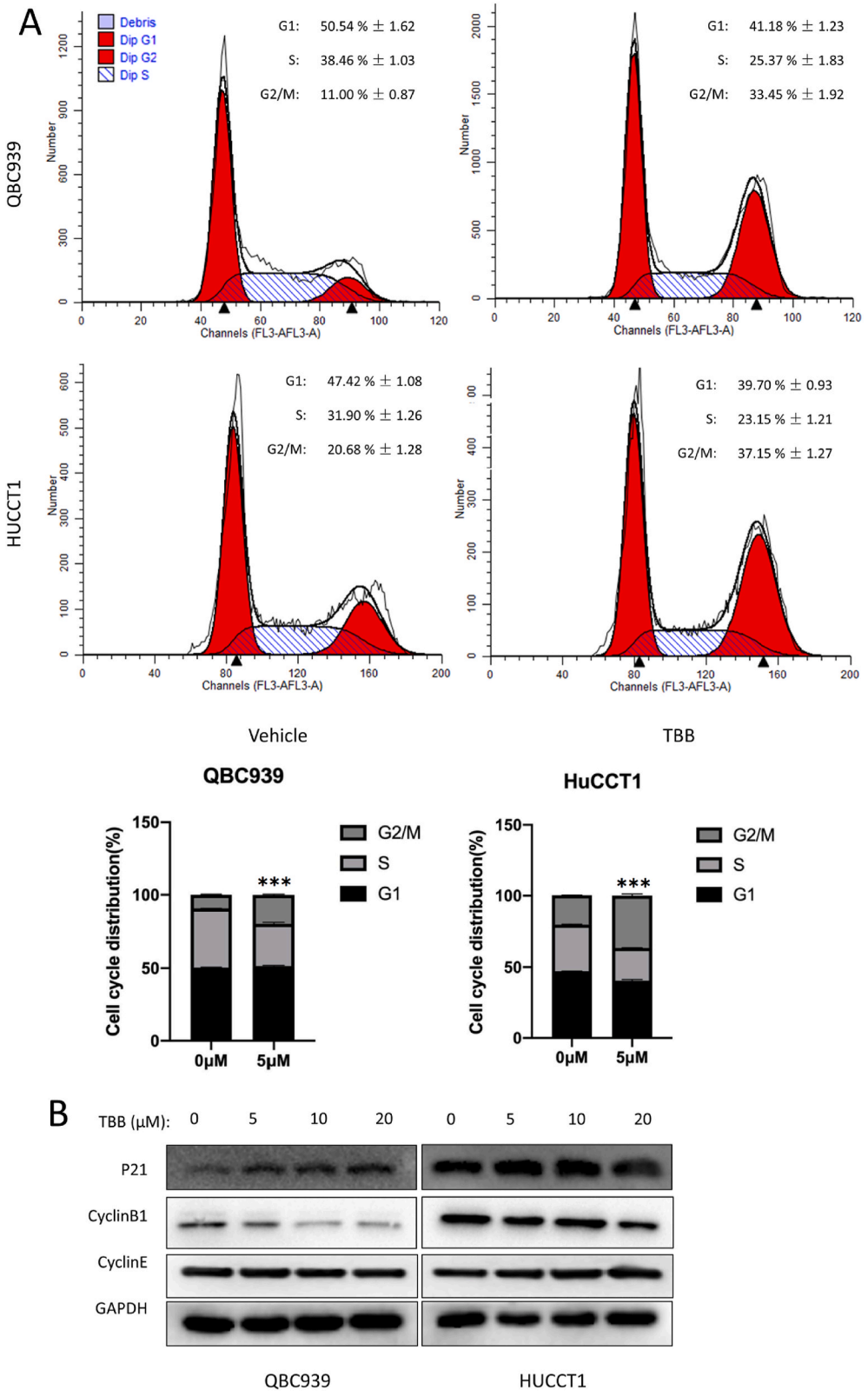

(caption on next page)

Fig. 4. Effect of TBB on cell cycle arrest was analyzed in CCA cells
(A) Flow cytometry was used to analyze cell cycle distribution of QBC939 and HuCCT1 cells treated with TBB at 5 μM for 24 h. (B) The expression of cell cycle related proteins was detected by western blotting in the HuCCT1 and QBC939 cells treated by TBB at different concentrations (0 μM, 5 μM, 10 μM, and 20 μM) for 24 h.

2.14. Animal model

Nude mice (BALB/c, 14–16 g) were provided by the Shanghai Laboratory Animal Center. The mice (n = 18) were subcutaneously injected with QBC939 cells into the right armpit. The mice received an intraperitoneal injection of the drug when the tumor volume reached 60–100 mm3, and all the mice were randomly divided into three groups: TBB, 5FU, and vehicle groups. The two drugs, 5FU, and TBB were configured into the 10 μM solution for subsequent chemotherapy. The TBB, 5FU, and vehicle treatment groups were administered 20 mg/kg of TBB (every two days, n = 6), 30 mg/kg of 5FU (every two days, n = 6), and PBS (every two days, n = 6), respectively. Tumor volume and body weight were recorded daily. After 12 drug treatments, all the mice were sacrificed. Tumor and normal tissues of the nude mice were collected, and further experiments were conducted on the samples. Tumor volume was calculated using the formula: $0.5 \times a \times b^2$ (a: Tumor Long Diameter; b: Tumor Short Diameter). All animal experiments were approved by The Animal Ethics Committee of Xiamen University (approval number: XMULAC20180077).

2.15. Immunohistochemistry and Hematoxylin–Eosin staining

The tumor tissues were fixed in 10% neutral formalin and embedded in paraffin. Approximately 4 μm sections of paraffin were cut and baked at 65 °C for 4 h. The baked pieces were placed in an environmentally friendly transparent agent containing 100% alcohol, 95% alcohol, and 75% alcohol for dewaxing.

Tissue sections were placed in a citric acid tissue antigen repair solution at a ratio of 1–100 and repaired in an autoclave for 2 min. Subsequently, it was incubated with peroxidase blocker for 10 min, washed three times with PBS, and primary antibody incubated at 4 °C for 12 h was added. The reaction enhancer was incubated at 37 °C for 20 min, and the secondary antibody was incubated for 30 min, followed by DAB staining for 1–3 min during microscopic observation and hematoxylin staining for 1 min.

For hematoxylin and eosin staining, the sections were washed under running water for 10 min after dewaxing. They were then stained with hematoxylin for 1 min and eosin for 1–2 min.

At the end of the staining, the pieces were dehydrated and sealed with neutral tree glue. The morphological characteristics of the tumor tissues were examined using a Nikon microscope.

2.16. Statistical analysis

Data were collected from three repeated experiments, and all the data were expressed and calculated as means ± standard error of the mean (S.E.M). Statistical analyses were performed using GraphPad Prism 8.0 (CA, USA). Group comparisons were assessed using Student's t-test, and p-values <0.05 were considered statistically significant.

3. Results

3.1. TBB inhibited the proliferation and colony formation of CCA cells

To evaluate the effects of TBB on CCA cell proliferation, the QBC939 cells were treated with different concentrations of TBB, 5-FU, CDDP, TAX, or LHOP for 24 h. The MTS assay results indicated that the percentage of cell survival after treatment with TBB was lower than that in the other four drug-treated groups *in vitro* (Fig. 2A). The IC50 of TBB was the lowest among the five drugs tested (Fig. 2B). MZ-ChA-1, HuCCT1, QBC939, and TFK1 cells were treated with different concentrations and times, respectively. The data confirmed that the percentage of surviving cells decreased as the concentration and duration of TBB treatment increased. The TBB inhibited CCA cell proliferation in a dose- and time-dependent manner (Fig. 2C). Additionally, the colony formation assay demonstrated that TBB significantly reduced the number of colonies in HuCCT1 and QBC939 cells compared to the vehicle groups. The rate of TBB inhibition was >80% and >70% in HuCC1 and QBC939 cells, respectively (Fig. 2D).

Simultaneously, the amount of DNA synthesis, as indicated by Hoechst 33,258 and EdU staining, was detected in the CCA cells to reveal the effect of TBB on proliferation. The results showed a remarkable reduction in the quantity of blue and red fluorescence in the TBB groups compared to that in the vehicle groups in HuCCT1 and QBC939 cells (Fig. 3A). The expression of the proliferation markers, Ki67 and PCNA, was inhibited in a dose-dependent manner in HuCCT1 and QBC939 cells treated with TBB (Fig. 3B). These results indicated that TBB inhibited cell proliferation and colony formation in CCA cells.

3.2. TBB arrested the cell cycles at G2/M phase in CCA cells

Cell proliferation is closely associated with cell cycle progression. To investigate the role of TBB in CCA cells, FCM was used to assess the cell cycle distribution. These findings revealed a significant change in the distribution of cell cycle phases in both the QBC939 and HuCCT1 cells treated with TBB for 24 h.

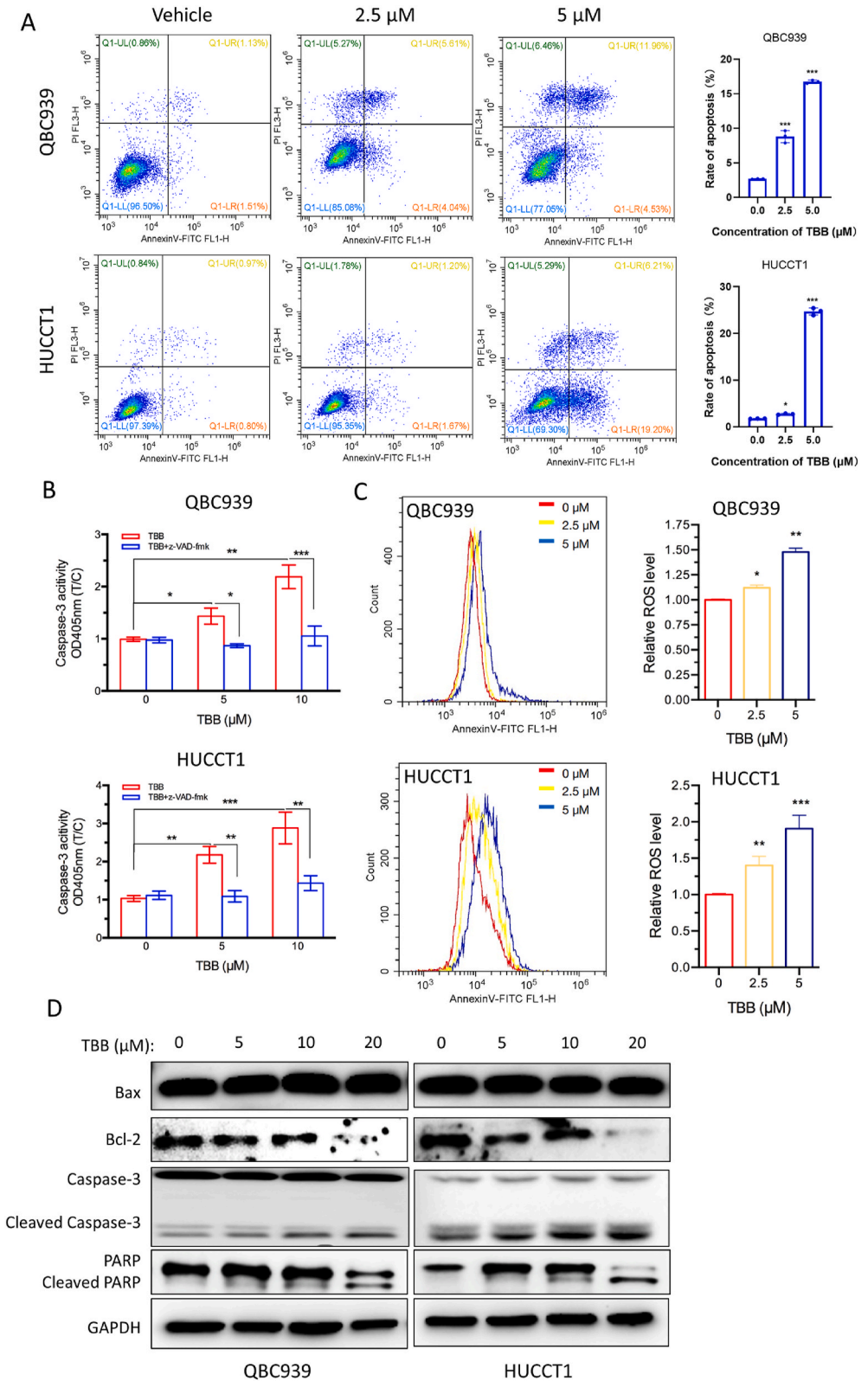

(caption on next page)

Fig. 5. TBB promoted apoptosis through mitochondrial pathway
(A) FCM was used to identify the rate of cell apoptosis by Annexin V-FITC/PI staining. (B) Caspase-3 activity of QBC939 and HuCCT1 cells was detected with or without z-VAD-fmk in the presence of TBB at different concentrations (5 μM and 10 μM) for 24 h. (C) ROS levels of QBC939 and HuCCT1 cells were detected by flow cytometry at different concentrations (2.5 μM and 5 μM) of TBB for 24 h. (D) Western blotting was used to examine the expression of apoptosis related protein in QBC939 and HuCCT1 cells treated with TBB at various concentrations (0 μM, 5 μM, 10 μM, and 20 μM) for 24 h. Data values were expressed as mean ± SEM of three independent experiments. *P < 0.05, **P < 0.01, and ***P < 0.001.

Specifically, the ratio of cells in the G1 phase decreased from 50.54% ± 1.62–41.18% ± 1.23 and from 47.42% ± 1.08–39.70% ± 0.93 in the QBC939 and HuCCT1 cells, respectively. Additionally, the proportion of cells in the S phase decreased from 38.46% ± 1.03–25.37% ± 1.83 and from 31.90% ± 1.26–23.15% ± 1.21 in the QBC939 and HuCCT1 cells, respectively. Furthermore, the percentage of cells in the G2/M phase increased from 11% ± 0.87–33.45% ± 1.92 and from 20.68% ± 1.28–37.15% ± 1.27 in the QBC939 and HuCCT1 cells, respectively (Fig. 4A).

In summary, treatment with TBB significantly altered the distribution of cell cycle phases in the CCA cells, resulting in a decrease in the proportion of cells in the G1 and S phases, and an increase in the proportion of cells in the G2/M phase. This indicated that TBB effectively arrested the cell cycle of CCA cells at the G2/M phase.

Moreover, the expression of cyclin B1, an essential factor for G2/M phase transition, was reduced, whereas the expression of the cell cycle inhibitor, P21, was increased in both the HuCCT1 and QBC939 cells treated with TBB. Additionally, the expression of cyclin E increased in the QBC939 cells treated with TBB, although no significant change was observed in the HuCCT1 cells (Fig. 4B). Based on these results, it can be inferred that TBB induces cell cycle arrest in the G2/M phase in CCA cells.

3.3. TBB induced apoptosis of CCA cells

Chemotherapeutic drugs effectively induce apoptosis, a key mechanism of programmed cell death in tumor cells. In our experiment, we used FCM to assess the effect of TBB on the apoptosis of CCA cells. Treatment with TBB resulted in a noticeable increase in the apoptotic rate of both the QBC939 and HuCCT1 cells compared to that in the vehicle group. Additionally, the apoptotic rate was higher at a concentration of 5 μM than 2.5 μM for the TBB treatment in both cell lines (Fig. 5A). To investigate the involvement of caspase-3 in TBB-induced apoptosis, we measured its activity in QBC939 and HuCCT1 cells treated with or without the apoptosis inhibitor z-VAD-fmk in the presence of TBB. Our data demonstrated that the activity of caspase-3 was stronger in the TBB group than that in the control group, and this effect was completely reversed by z-VAD-fmk treatment (Fig. 5B). Furthermore, we employed Annexin V-FITC/PI staining and FCM to evaluate mitochondrial damage and the subsequent production of ROS. Following the incubation with TBB at concentrations of 2.5 μM and 5 μM, the levels of intracellular ROS were significantly increased in the TBB group compared to those in the vehicle group, with a more pronounced increase observed at 5 μM than 2.5 μM in both the QBC939 and HuCCT1 cells (Fig. 5C). The mitochondrial pathway plays a crucial role in apoptosis. In QBC939 and HuCCT1 cells treated with different concentrations of TBB, the cleaved forms of PARP and caspase-3 were upregulated, whereas Bcl-2 was downregulated, as evidenced by Western blot analysis (Fig. 5D).

In further research, Hoechst staining and AO/EB staining were employed to observe cell apoptosis of QBC939 cells and HuCCT1 cells which were treated with TBB at 2.5 μM and 5 μM for 24 h. The results showed that TBB increased apoptosis in HUCCT1 and QBC939 cells (Figure S1A-C, Figure S1 is the supplementary figure to Fig. 5). Overall, these data suggested that TBB enhanced oxidative stress and promoted apoptosis through mitochondrial pathway in CCA cells.

3.4. TBB inhibited CCA xenograft tumor growth in vivo

In this study, QBC939 cells were used to establish a xenograft tumor model in nude mice to investigate the antitumor effects of TBB *in vivo*. Both normal and tumor tissues were collected from the mice to assess the cytotoxicity and specificity of TBB. The data demonstrated that TBB did not induce any changes in the histology (Fig. 6A) or weight (Fig. 6B) of vital organs, including the heart, liver, kidney, spleen, and lung. Additionally, there were no significant changes in body weight (Fig. 6C) between the TBB treatment group and vehicle group. Tumor volume and weight were significantly reduced in TBB treatment group compared to those in the vehicle-treated group. Moreover, the inhibition of tumor growth by TBB was more potent than that of 5-FU (Fig. 6D–F). We further observed the histomorphology of the transplanted tumors and found that the cells in the control group were large, and the nuclei were well arranged, whereas in the TBB- and 5FU-treated groups, the nuclei were dispersed (Fig. 6G). Furthermore, immunohistochemical analysis revealed that the expression of proliferation markers, PCNA and Ki67, was lower in the TBB treatment group than that in the vehicle-treated group (Fig. 6G). Thus, our findings indicated that TBB specifically inhibited the proliferation of CCA cells both *in vivo and in vitro* studies.

3.5. TBB exerted its anti-tumor effect via JAK/STAT3 signaling pathway regulation

The JAK/STAT3 signaling pathway was related to cell proliferation and apoptosis, and the effect of TBB on the JAK/STAT3 signaling pathway was detected by western blotting. Compared with the control group, IL-6 promoted the phosphorylation of STAT3 in QBC939 and HuCCT1 cells, and this positive effect was inhibited by TBB (Fig. 7A). At the same time, TBB inhibited the upregulation of PCNA and Bcl-2 and downregulation of P21 induced by IL-6 (Fig. 7B). Consequently, TBB prevented the proliferation and induced the

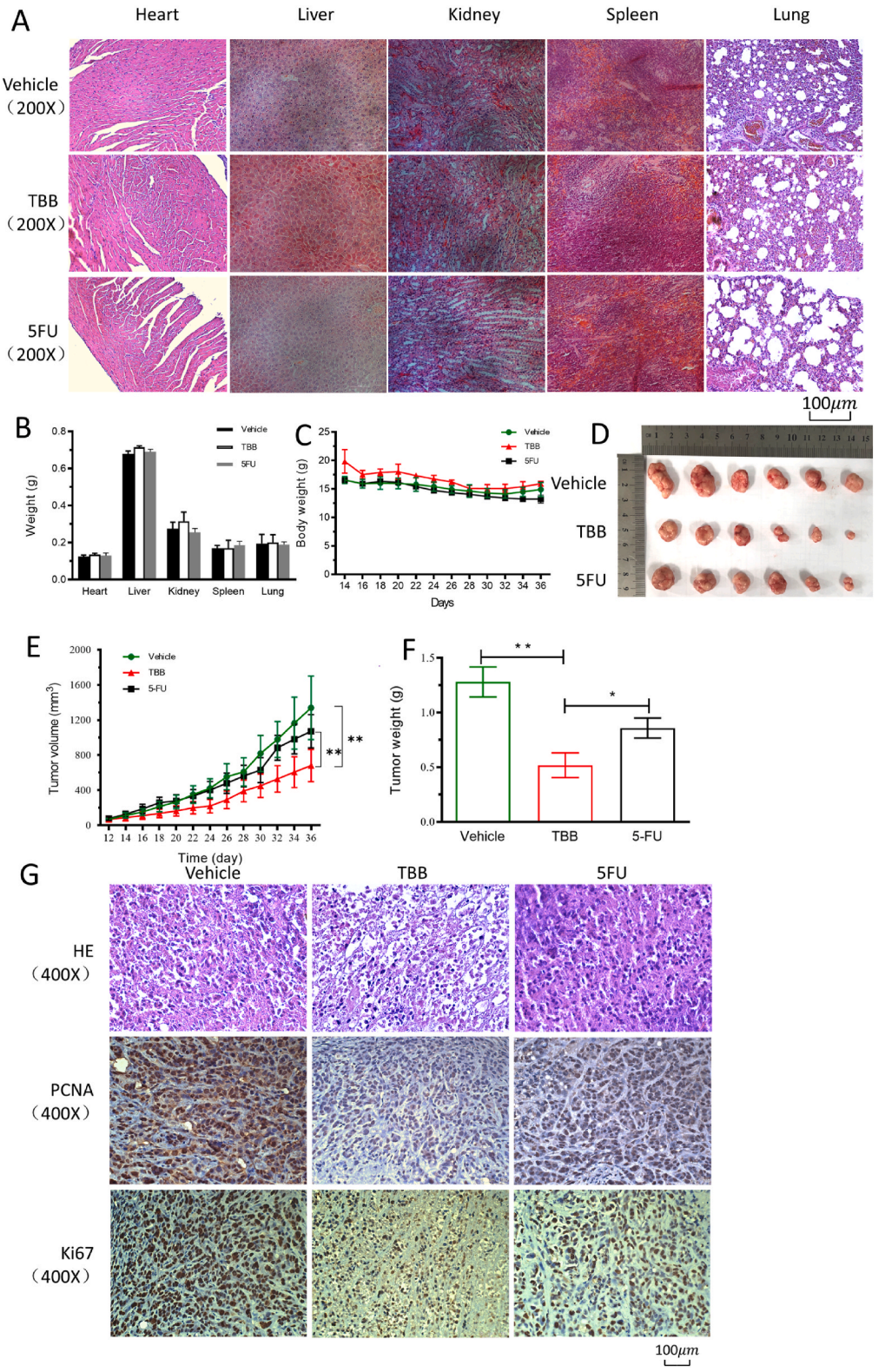

Fig. 6. TBB inhibited the growth of xenograft tumor *in vivo*.
QBC939 cells were subcutaneously injected into nude mice, which were randomly divided into three groups and treated with TBB and 5-FU every two days by intraperitoneal injection when the tumor volume grew to 60–100 mm3. The nude mice were euthanized after 12 intraperitoneal injections of TBB. (A) H&E staining and (B) weights of the heart, liver, kidney, spleen, and lung in mice in the TBB, 5-FU and vehicle groups. (C) Body

weight of the nude mice in the TBB, 5-FU, and vehicle groups were recorded. (D) General observations, (E) volume, and (F) weight of the xenograft tumors in the nude mice were compared in the TBB, 5FU, and vehicle groups. (G) H&E and IHC staining of the nude mice xenograft tumor tissues. Data values were expressed as mean ± SEM of three independent experiments. *P < 0.05, **P < 0.01, and ***P < 0.001.

apoptosis of CCA cells, by potentially suppressing the activation of STAT3 transcription; that is, TBB played an antitumor role by inhibiting the JAK/STAT3 signaling pathway (Fig. 7C).

4. Discussion

Given the poor prognosis and high mortality associated with CCA, there is an urgent need to identify novel chemotherapeutic drugs. The use of natural products for the discovery of new drugs has a long history [38]. Here, we demonstrate for the first time that TBB exerts an antitumor effect in CCA. As an extract of *Wedelia trilobata*, in our study, TBB significantly suppresses the proliferation of CCA cells and promotes their apoptosis both *in vitro and in vivo*. Furthermore, TBB downregulates PCNA and Bcl-2 expression, while upregulating P21 expression at the protein level through the promotion of STAT3 phosphorylation. Overall, our findings indicates that TBB exerts its antitumor effects by inhibiting the JAK-STAT3 pathway in CCA cells.

In drug research, evaluating the efficacy of drugs by examining their ability to arrest the cell cycle is an effective method [39]. For example, *Silibinin* improves the treatment of various cancers by acting as a cell cycle inhibitor [40]. Similarly, *Dihydroartemisinin* arrests the cell cycle and induces apoptosis of CCA cells [41]. In a separate study, four *Wedelia trilobata* extracts show not only cell proliferation inhibition and apoptosis acceleration but also cell cycle arrest in prostate cancer cells [42]. In our study, TBB arrests the cell cycle at the G2/M phase in the QBC939 and HuCCT1 cells, similar to other extracts; however, the underlying mechanism needs to be further explored.

A previous study demonstrated that numerous drugs were developed to specifically target mitochondria, which served as crucial regulators of cellular processes and played a significant role in cancer treatment [43]. Trilobolide-6-O-isobutyrate boosts the production of ROS, thereby inducing oxidative stress reactions and increasing the Bax/Bcl-2 ratio to activate mitochondria-mediated apoptosis in CCA cells. This aligns with a previous study in which *Betulinic acid* was found to induce apoptosis in differentiated PC12 cells by activating the ROS-mediated mitochondrial pathway [44].

Trilobolide-6-O-isobutyrate effectively inhibited the growth of xenograft tumors in nude mice. 5-Fluorouracil, a thymidylate synthase inhibitor, is the first-line chemotherapeutic drug for the treatment of CCA. However, their clinical application is limited by the development of severe drug resistance [45,46]. Therefore, it is necessary to develop new chemotherapeutic drugs for CCA treatment. In our study, TBB demonstrates superior efficacy compared to 5-FU. Evidence reveals that xenograft tumor mice treated with TBB display smaller tumor volumes and lower tumor weights than those treated with 5-FU.

The JAK/STAT3 signaling pathway is widely recognized for its role in the regulation of cell growth, proliferation, and apoptosis [47–50]. Increasing evidence suggests that dysregulation of the JAK/STAT3 pathway is implicated in various cancers, making it a prime target for the antitumor effects of numerous drugs [51–54], such as *Banxia xiexin decoction* [55], *Curcumin* [56] and *Triptolide* [57]. In this study, TBB effectively inhibits the progression of CCA by suppressing the phosphorylation of STAT3. Additionally, it regulates tumor growth by modulating the transcription of key genes involved in cell proliferation and apoptosis [52]. Particularly, TBB decreases PCNA expression, downregulates the Bcl-2/Bax ratio, and increases the expression P21 by inhibiting STAT3 pathway activation. These findings suggest that TBB exerts its antitumor effects by targeting the JAK/STAT3 signaling pathway, making it a potential chemotherapeutic agent for CCA and improving patient prognosis.

5. Conclusions

We demonstrate the antitumor efficacy of TBB against CCA *in vitro* and *in vivo*. Mechanistically, TBB suppresses the proliferation of CCA cells and triggers apoptosis by inhibiting the JAK/STAT3 signaling pathway. Our findings indicate that TBB holds promise as a potent chemotherapeutic agent, thereby offering a potential pathway for enhancing CCA treatment.

Ethics Declarations.

This study is reviewed and approved by the Animal Ethics Committee of Xiamen University (approval number: XMULAC20180077).

Data availability statement

Data will be made available on request.

CRediT authorship contribution statement

Hao-Xuan Zhang: Writing – review & editing, Writing – original draft, Methodology, Investigation. **Rui Fan:** Writing – original draft, Visualization. **Qian-En Chen:** Validation, Software. **Lin-Jun Zhang:** Investigation. **Yang Hui:** Visualization. **Peng Xu:** Formal analysis. **Si-Yang Li:** Formal analysis. **Guang-Ying Chen:** Resources, Project administration, Data curation. **Wen-Hao Chen:** Resources, Project administration, Funding acquisition. **Dong-Yan Shen:** Resources, Funding acquisition, Conceptualization.

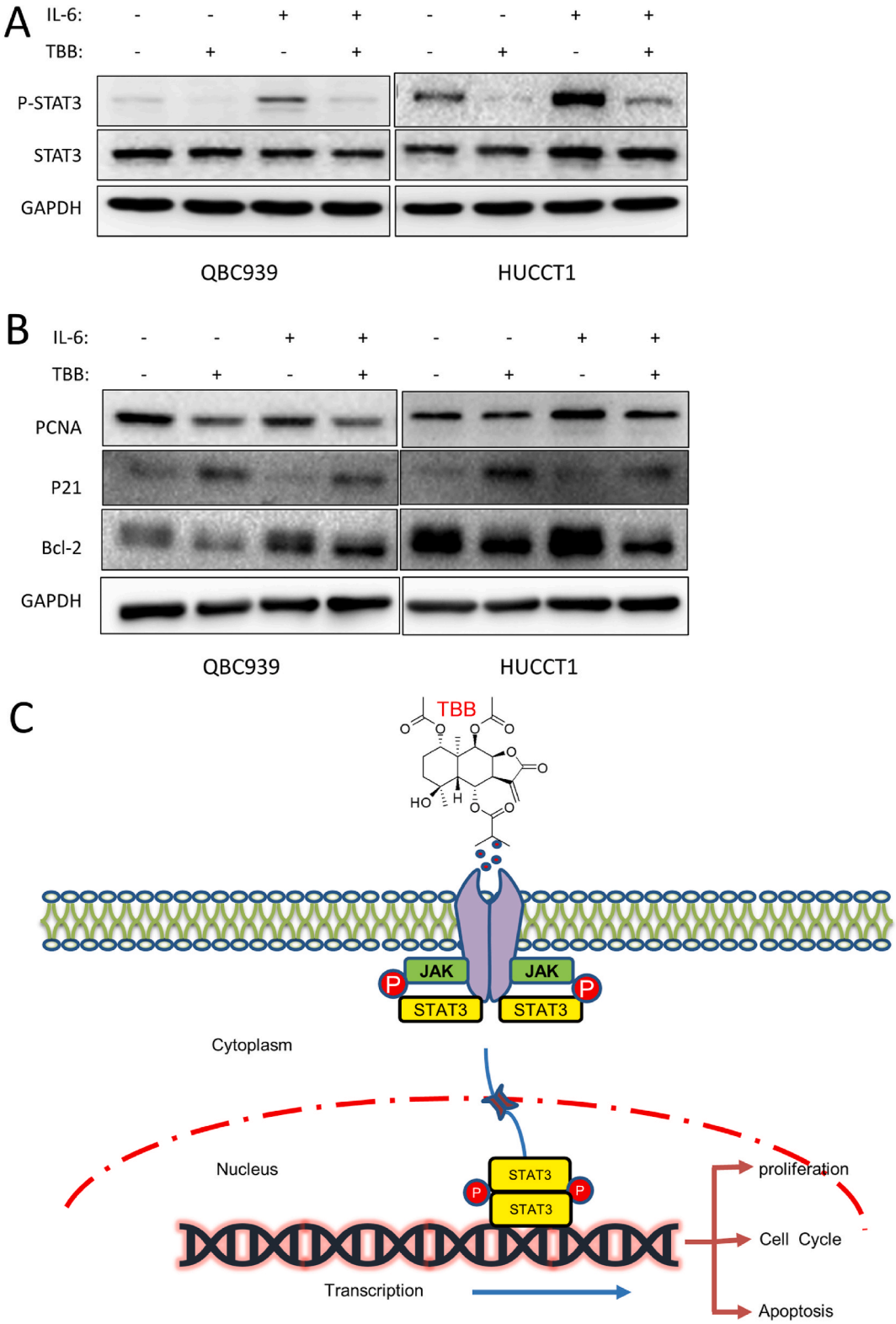

Fig. 7. Potential mechanism of TBB was explored in CCA cells
(A) STAT3 phosphorylation, and (B) PCNA, P21, and Bcl-2 expression by western blotting in QBC939 and HuCCT1 cells treated with TBB and/or IL-6. (C) Schematic diagram of TBB versus CCA.

Declaration of competing interest

The authors declare that they have no known competing financial interests or personal relationships that could have appeared to influence the work reported in this paper.

Acknowledgments

This study is supported by the National Natural Science Foundation of China (Grant Nos. 82270664 and 22167013) , the Project of Xiamen Cell Therapy Research Center, Xiamen, Fujian, China (Grant No.3502Z20214001) and Key Project of Research and Development of Hainan Province (ZDYF2021SHFZ221).

Appendix A. Supplementary data

Supplementary data to this article can be found online at https://doi.org/10.1016/j.heliyon.2024.e27217.

References

[1] N. Razumilava, G.J. Gores, Cholangiocarcinoma, Lancet 383 (9935) (2014) 2168–2179.
[2] S. Rizvi, S.A. Khan, C.L. Hallemeier, et al., Cholangiocarcinoma - evolving concepts and therapeutic strategies, Nat. Rev. Clin. Oncol. 15 (2) (2018) 95–111.
[3] L.B. Alexandrov, S. Nik-Zainal, D.C. Wedge, et al., Signatures of mutational processes in human cancer, Nature 500 (7463) (2013) 415–421.
[4] S. Petmitr, S. Pinlaor, A. Thousungnoen, et al., K-ras oncogene and p53 gene mutations in cholangiocarcinoma from Thai patients, Southeast Asian J. Trop. Med. Publ. Health 29 (1) (1998) 71–75.
[5] L. Fabris, K. Sato, G. Alpini, et al., The tumor microenvironment in cholangiocarcinoma progression, Hepatology 73 (Suppl 1) (2021) 75–85. Suppl 1.
[6] C. Louis, J. Edeline, C. Coulouarn, Targeting the tumor microenvironment in cholangiocarcinoma: implications for therapy, Expert Opin. Ther. Targets 25 (2) (2021) 153–162.
[7] S. Rizvi, M.J. Borad, The rise of the FGFR inhibitor in advanced biliary cancer: the next cover of time magazine? J. Gastrointest. Oncol. 7 (5) (2016) 789–796.
[8] Y. Arai, Y. Totoki, F. Hosoda, et al., Fibroblast growth factor receptor 2 tyrosine kinase fusions define a unique molecular subtype of cholangiocarcinoma, Hepatology 59 (4) (2014) 1427–1434.
[9] A. Pellat, J. Vaquero, L. Fouassier, Role of ErbB/HER family of receptor tyrosine kinases in cholangiocyte biology, Hepatology 67 (2) (2018) 762–773.
[10] A. Claperon, N. Guedj, M. Mergey, et al., Loss of EBP50 stimulates EGFR activity to induce EMT phenotypic features in biliary cancer cells, Oncogene 31 (11) (2012) 1376–1388.
[11] A. Claperon, M. Mergey, T.H. Nguyen Ho-Bouldoires, et al., EGF/EGFR axis contributes to the progression of cholangiocarcinoma through the induction of an epithelial-mesenchymal transition, J. Hepatol. 61 (2) (2014) 325–332.
[12] J.M. Banales, J.J.G. Marin, A. Lamarca, et al., Cholangiocarcinoma 2020: the next horizon in mechanisms and management, Nat. Rev. Gastroenterol. Hepatol. 17 (9) (2020) 557–588.
[13] N. Barner-Rasmussen, E. Pukkala, K. Hadkhale, et al., Risk factors, epidemiology and prognosis of cholangiocarcinoma in Finland, United European Gastroenterol J 9 (10) (2021) 1128–1135.
[14] L. Fouassier, M. Marzioni, M.B. Afonso, et al., Signalling networks in cholangiocarcinoma: molecular pathogenesis, targeted therapies and drug resistance, Liver Int. 39 (Suppl 1) (2019) 43–62.
[15] X.R. Baskaran, A.V. Geo Vigila, S.Z. Zhang, et al., A review of the use of pteridophytes for treating human ailments, J. Zhejiang Univ. - Sci. B 19 (2) (2018) 1–35.
[16] E.I.M.M. Saleh, A. Roy, M.A. AL-Mansur, et al., Isolation and in silico prediction of potential drug-like compounds from Anethum sowa L. root extracts targeted towards cancer therapy, Comput. Biol. Chem. 78 (2019) 242–259.
[17] G. Babaei, A. Aliarab, S. Abroon, et al., Application of sesquiterpene lactone: a new promising way for cancer therapy based on anticancer activity, Biomed. Pharmacother. 106 (2018) 239–246.
[18] C.H. Tsai, F.M. Lin, Y.C. Yang, et al., Herbal extract of Wedelia chinensis attenuates androgen receptor activity and orthotopic growth of prostate cancer in nude mice, Clin. Cancer Res. 15 (17) (2009) 5435–5444.
[19] J. Yang, J.A. Yoon, K. Kim, et al., The first synthesis and immunomodulatory properties of p-hydroxyphenyl caffeate derived from Wedelia trilobata, J. Asian Nat. Prod. Res. 22 (10) (2020) 966–975.
[20] L. Sun, Z. Wang, Y. Wang, et al., Anti-proliferative and anti-neuroinflammatory eudesmanolides from Wedelia (sphagneticola trilobata (L.) pruski), Fitoterapia 142 (2020) 104452.
[21] N.T. Luyen, P.T. Binh, P.T. Tham, et al., Wedtrilosides A and B, two new diterpenoid glycosides from the leaves of Wedelia trilobata (L.) Hitchc. with alpha-amylase and alpha-glucosidase inhibitory activities, Bioorg. Chem. 85 (2019) 319–324.
[22] X. Li, M. Dong, Y. Liu, et al., Structures and biological properties of the chemical constituents from the genus Wedelia, Chem. Biodivers. 4 (5) (2007) 823–836.
[23] A. Verma, D. Singh, F. Anwar, et al., Triterpenoids principle of Wedelia calendulacea attenuated diethynitrosamine-induced hepatocellular carcinoma via down-regulating oxidative stress, inflammation and pathology via NF-kB pathway, Inflammopharmacology 26 (1) (2018) 133–146.
[24] X. Huang, S. Ou, S. Tang, et al., Simultaneous determination of trilobolide-6-O-isobutyrates A and B in Wedelia trilobata by gas chromatography, Se Pu 24 (5) (2006) 499–502.
[25] X.Q. Zhou, X.M. Mao, R. Fan, et al., Trilobolide-6-O-isobutyrate suppresses hepatocellular carcinoma tumorigenesis through inhibition of IL-6/STAT3 signaling pathway, Phytother Res. 35 (10) (2021) 5741–5753.
[26] Y. Hui, J. Cao, J. Lin, et al., Eudesmanolides and other constituents from the flowers of Wedelia trilobata, Chem. Biodivers. 15 (3) (2018) e1700411.
[27] P. Han, J. Shang, D.-L. Chen, et al., Baicalein mediates anticancer effect on cholangiocarcinoma through co-targeting the AKT/NF-κB and STAT3 signaling pathway, Process Biochem. 102 (2021) 304–314.
[28] F.Q. Wang, E.V. Ariztia, L.R. Boyd, et al., Lysophosphatidic acid (LPA) effects on endometrial carcinoma in vitro proliferation, invasion, and matrix metalloproteinase activity, Gynecol. Oncol. 117 (1) (2010) 88–95.
[29] S.-Y. Li, J. Shang, X.-M. Mao, et al., Diosgenin exerts anti-tumor effects through inactivation of cAMP/PKA/CREB signaling pathway in colorectal cancer, Eur. J. Pharmacol. (2021) 908.
[30] Q. Zhang, J. Liu, S. Chen, et al., Caspase-12 is involved in stretch-induced apoptosis mediated endoplasmic reticulum stress, Apoptosis 21 (4) (2016) 432–442.
[31] S. Liu, W. Li, M. Xu, et al., Micro-RNA 21 Targets dual specific phosphatase 8 to promote collagen synthesis in high glucose-treated primary cardiac fibroblasts, Can. J. Cardiol. 30 (12) (2014) 1689–1699.
[32] S. Sun, T. Gao, B. Pang, et al., RNA binding protein NKAP protects glioblastoma cells from ferroptosis by promoting SLC7A11 mRNA splicing in an m(6)A-dependent manner, Cell Death Dis. 13 (1) (2022) 73.

[33] W. Wang, J. Chen, D. Hu, et al., SARS-CoV-2 N protein induces acute kidney injury via smad3-dependent G1 cell cycle arrest mechanism, Adv. Sci. 9 (3) (2022) e2103248.
[34] L. Wang, T. Hu, Z. Shen, et al., Inhibition of USP1 activates ER stress through Ubi-protein aggregation to induce autophagy and apoptosis in HCC, Cell Death Dis. 13 (11) (2022) 951.
[35] D. Xu, L. Liu, Y. Zhao, et al., Melatonin protects mouse testes from palmitic acid-induced lipotoxicity by attenuating oxidative stress and DNA damage in a SIRT1-dependent manner, J. Pineal Res. 69 (4) (2020) e12690.
[36] J. Xiong, J. He, J. Zhu, et al., Lactylation-driven METTL3-mediated RNA m(6)A modification promotes immunosuppression of tumor-infiltrating myeloid cells, Mol. Cell. 82 (9) (2022) 1660, 77.e10.
[37] H. Bera, Y.F. Abbasi, V. Gajbhiye, et al., Carboxymethyl fenugreek galactomannan-g-poly(N-isopropylacrylamide-co-N,N'-methylene-bis-acrylamide)-clay based pH/temperature-responsive nanocomposites as drug-carriers, Mater. Sci. Eng., C 110 (2020) 110628.
[38] T. Rodrigues, D. Reker, P. Schneider, et al., Counting on natural products for drug design, Nat. Chem. 8 (6) (2016) 531–541.
[39] J. Liu, Y. Peng, W. Wei, Cell cycle on the crossroad of tumorigenesis and cancer therapy, Trends Cell Biol. 32 (1) (2022) 30–44.
[40] Z. Jahanafrooz, N. Motamed, B. Rinner, et al., Silibinin to improve cancer therapeutic, as an apoptotic inducer, autophagy modulator, cell cycle inhibitor, and microRNAs regulator, Life Sci. 213 (2018) 236–247.
[41] S. Thongchot, C. Vidoni, A. Ferraresi, et al., Dihydroartemisinin induces apoptosis and autophagy-dependent cell death in cholangiocarcinoma through a DAPK1-BECLIN1 pathway, Mol. Carcinog. 57 (12) (2018) 1735–1750.
[42] F.M. Lin, L.R. Chen, E.H. Lin, et al., Compounds from Wedelia chinensis synergistically suppress androgen activity and growth in prostate cancer cells, Carcinogenesis 28 (12) (2007) 2521–2529.
[43] J.S. Armstrong, Mitochondria-directed therapeutics, Antioxidants Redox Signal. 10 (3) (2008) 575–578.
[44] X. Wang, X. Lu, R. Zhu, et al., Betulinic acid induces apoptosis in differentiated PC12 cells via ROS-mediated mitochondrial pathway, Neurochem. Res. 42 (4) (2017) 1130–1140.
[45] K. Intuyod, P. Saavedra-GarcíA, S. Zona, et al., FOXM1 modulates 5-fluorouracil sensitivity in cholangiocarcinoma through thymidylate synthase (TYMS): implications of FOXM1-TYMS axis uncoupling in 5-FU resistance, Cell Death Dis. 9 (12) (2018) 1185.
[46] N. Klinhom-On, W. Seubwai, K. Sawanyawisuth, et al., FOXM1 inhibitor, Siomycin A, synergizes and restores 5-FU cytotoxicity in human cholangiocarcinoma cell lines via targeting thymidylate synthase, Life Sci. 286 (2021) 120072.
[47] F. Zhang, L. Li, X. Yang, et al., Expression and activation of EGFR and STAT3 during the multistage carcinogenesis of intrahepatic cholangiocarcinoma induced by 3'-methyl-4 dimethylaminoazobenzene in rats, J. Toxicol. Pathol. 28 (2) (2015) 79–87.
[48] H. Dokduang, A. Techasen, N. Namwat, et al., STATs profiling reveals predominantly-activated STAT3 in cholangiocarcinoma genesis and progression, J Hepatobiliary Pancreat Sci 21 (10) (2014) 767–776.
[49] H. Isomoto, S. Kobayashi, N.W. Werneburg, et al., Interleukin 6 upregulates myeloid cell leukemia-1 expression through a STAT3 pathway in cholangiocarcinoma cells, Hepatology 42 (6) (2005) 1329–1338.
[50] X.W. Yang, L. Li, G.J. Hou, et al., STAT3 overexpression promotes metastasis in intrahepatic cholangiocarcinoma and correlates negatively with surgical outcome, Oncotarget 8 (5) (2017) 7710–7721.
[51] X. Hu, J. Li, M. Fu, et al., The JAK/STAT signaling pathway: from bench to clinic, Signal Transduct. Targeted Ther. 6 (1) (2021) 402.
[52] D.E. Johnson, R.A. O'Keefe, J.R. Grandis, Targeting the IL-6/JAK/STAT3 signalling axis in cancer, Nat. Rev. Clin. Oncol. 15 (4) (2018) 234–248.
[53] U. Bharadwaj, M.M. Kasembeli, P. Robinson, et al., Targeting janus kinases and signal transducer and activator of transcription 3 to treat inflammation, fibrosis, and cancer: rationale, progress, and caution, Pharmacol. Rev. 72 (2) (2020) 486–526.
[54] H. Yu, H. Lee, A. Herrmann, et al., Revisiting STAT3 signalling in cancer: new and unexpected biological functions, Nat. Rev. Cancer 14 (11) (2014) 736–746.
[55] X. Feng, F. Xue, G. He, et al., Banxia xiexin decoction affects drug sensitivity in gastric cancer cells by regulating MGMT expression via IL-6/JAK/STAT3-mediated PD-L1 activity, Int. J. Mol. Med. 48 (2) (2021).
[56] A.Q. Khan, E.I. Ahmed, N. Elareer, et al., Curcumin-mediated apoptotic cell death in papillary thyroid cancer and cancer stem-like cells through targeting of the JAK/STAT3 signaling pathway, Int. J. Mol. Sci. 21 (2) (2020).
[57] Z. Wang, H. Jin, R. Xu, et al., Triptolide downregulates Rac 1 and the JAK/STAT3 pathway and inhibits colitis-related colon cancer progression, Exp. Mol. Med. 41 (10) (2009) 717–727.